Video Article

Determination of the Excitation and Coupling Rates Between Light Emitters and Surface Plasmon Polaritons

Zhaolong Cao[1,2], Min Lin[2], Daniel Ong[2]

[1]State Key Laboratory of Optoelectronic Materials and Technologies and Guangdong Province Key Laboratory of Display Material and Technology, School of Physics and Engineering, Sun Yat-sen University

[2]Department of Physics, The Chinese University of Hong Kong

Correspondence to: Daniel Ong at hcong@phy.cuhk.edu.hk

URL: https://www.jove.com/video/56735
DOI: doi:10.3791/56735

Keywords: Engineering, Issue 137, Photoluminescence, Periodic Arrays, Polarization-Resolved Spectroscopy, Fluorescence Enhancement, Surface Plasmon Mediated Fluorescence, Interference Lithography

Date Published: 7/21/2018

Citation: Cao, Z., Lin, M., Ong, D. Determination of the Excitation and Coupling Rates Between Light Emitters and Surface Plasmon Polaritons. *J. Vis. Exp.* (137), e56735, doi:10.3791/56735 (2018).

Abstract

We have developed a unique method to measure the excitation and coupling rates between the light emitters and surface plasmon polaritons (SPPs) arising from metallic periodic arrays without involving time-resolved techniques. We have formulated the rates by quantities that can be measured by simple optical measurements. The instrumentation based on angle- and polarization-resolved reflectivity and photoluminescence spectroscopy will be described in detail here. Our approach is intriguing due to its simplicity, which requires routine optics and several mechanical stages, and thus is highly affordable to most of the research laboratories.

Video Link

The video component of this article can be found at https://www.jove.com/video/56735/

Introduction

Surface plasmon mediated fluorescence (SPMF) has received considerable attention recently[1,2,3,4,5,6]. When light emitters are placed in close proximity to a plasmonic system, energy can be transferred between the emitters and surface plasmon polaritons (SPPs). In general, the strong plasmonic fields can strongly enhance the excitation of the emitters[2]. At the same time, the emission rate is also increased because of the large density-of-states created by SPPs, yielding the well-known Purcell effect[3]. These two processes work hand in hand in producing the SPMF. As SPMF has stimulated numerous applications in solid-state lighting[1,4], energy harvesting[5], and bio-detection[6], it is currently under intensive investigation. In particular, the knowledge of the energy transfer rates from the SPPs to the emitters and vice versa, *i.e.,* the excitation and coupling rates, is of great importance. However, the excitation and emission processes are usually entangled together, study on this aspect is still lacking. For example, most of the studies only determine the excitation efficiency ratio, which simply compares the emission with and without SPPs[7]. The exact measurement of the excitation rate is still missing. On the other hand, conventional time-resolved techniques such as fluorescence lifetime spectroscopy are routinely used for studying the dynamics of the emission process, but they are unable to separate the coupling rate from the total decay rate[8]. Here, we describe how one can determine them by combining the rate equation model and the temporal coupled mode theory[9,10]. Remarkably, we find that the excitation and coupling rates can be expressed in terms of measurable quantities, which can be accessed by performing angle- and polarization-resolved reflectivity and photoluminescence spectroscopy. We will first outline the formulation and then describe the instrumentation in detail. This approach is entirely frequency domain based and it does not require any time-resolved accessories such as ultra-fast lasers and time-correlated single-photon counters, which are expensive and sometimes difficult to implement[8,11]. We anticipate this technique to be an enabling technology for determining the excitation and coupling rates between light emitters and resonant cavities.

The SPMF in periodic systems is briefed here. For a periodic plasmonic system where Bloch-like SPPs can be generated, other than direct excitation and emission, which are characterized by the excitation efficiency η and spontaneous emission rate Γ_r, the emitters can be excited by incoming SPPs and decay via outgoing SPPs. In other words, under resonance excitation, incoming SPPs are generated to create strong plasmonic fields that energize the emitters. Once the emitters are excited, energy from them can be transferred to outgoing SPPs, which subsequently radiatively dissipate to far-field, giving rise to enhanced emission. They define SPMF. For simple two-level emitters, the excitation refers to the increased transition of electrons from the ground to the excited states whereas the emission defines the decay of electrons back to the ground states, accompanied by photon emission at wavelengths defined by the energy difference between the excited and ground states. The excitation and emission conditions for the SPMF are required to fulfill the well-known phase matching equation to excite the incoming and outgoing SPPs[9]

$$\frac{2\pi}{\lambda}\sqrt{\frac{\varepsilon_a\varepsilon_m}{\varepsilon_m+\varepsilon_a}} = \sqrt{\left(\frac{2\pi}{\lambda}\sin\theta\cos\varphi + \frac{2m\pi}{P}\right)^2 + \left(\frac{2\pi}{\lambda}\sin\theta\sin\varphi + \frac{2n\pi}{P}\right)^2} \quad (1)$$

where ε_a and ε_m are the dielectric constants of the dielectrics and the metal, θ and φ are the incident and azimuthal angles, P is the period of the array, λ is the excitation or emission wavelength, and m and n are the integers specifying the order of SPPs. For excitation, the in-plane wavevector of the laser beam will be Bragg scattered to momentum match with the incoming SPPs and the θ and φ together define the specified incident configuration for exciting the SPPs to enhance the electronic absorption at the excitation wavelength λ_{ex}. Likewise, for the emission, the outgoing SPPs will be reversely Bragg scattered to match with the light line and the angles now represent the possible emission channels at the emission wavelength λ_{em}. However, it is noted that as the emitters can couple their energy to vectorial propagating SPPs with $\vec{k}_{spp}$ that has the same magnitude $\left|\vec{k}_{spp}\right| = \frac{2\pi}{\lambda_{em}}\sqrt{\frac{\varepsilon_a\varepsilon_m}{\varepsilon_m+\varepsilon_a}}$ but different directions, the SPPs can decay via various combination of (m,n) to far-field following Eq. (1).

By using the rate equation model and temporal coupled mode theory (CMT), we find that the excitation rate Γ_{ex}, *i.e.,* the energy transfer rate from SPPs to emitters, can be expressed as[9,12,13]

$$\Gamma_{ex} = \eta\left(\frac{P_d^w}{P_d^{w/o}}\right)\frac{\Gamma_{tot}^2}{4\Gamma_{rad}} \quad (2)$$

where η is the aforementioned direct excitation rate in the absence of the incoming SPPs, Γ_{tot} is the total decay rate of the incoming SPPs $= \Gamma_{abs} + \Gamma_{rad} + \Gamma_{ex}$ in which Γ_{abs} and Γ_{rad} are the Ohmic absorption and radiative decay rates of SPPs, and $P_d^w/P_d^{w/o}$ is the photoluminescence power ratio with and without the incoming SPPs. On the other hand, the coupling rate Γ_c, *i.e.,* the energy transfer rate from emitters to SPPs, can be written as:

$$\Gamma_c^{\vec{k}_{spp}} = \Gamma_r\left(\frac{P_{SPP}^{\vec{k}_{spp},\alpha}}{P_d}\right)\left(\frac{\Gamma_{tot}}{\Gamma_{rad}^{\alpha}}\right) \quad (3)$$

where Γ_r is the direct emission rate, $P_{SPP}^{\vec{k}_{spp},\alpha}/P_d$ is the photoluminescence power ratio between the α^{th} SPP mediated decay and direct ports, and Γ_{rad}^{α} and Γ_{tot} are the radiative decay rates for the α^{th} port and the total decay rates. We will see that while all the SPP decay rates can be measured by reflectivity spectroscopy, the emission power ratio can be determined by photoluminescence spectroscopy. Details of the formulations can be found in reference[9,10].

Protocol

1. Setup of Interference Lithography

NOTE: Interference lithography is used to fabricate the periodic arrays[12]. The schematic setup, as is shown in **Figure 1**, is built up as follows:

1. Focus the 325 nm laser from a HeCd multimode laser to a 13X UV objective lens and pass it through a 50 μm pinhole based spatial filter for mode cleaning.
2. Place two 2.5 cm diameter irises 30 cm apart to further filter the central region of the diverging light. After the second iris, the beam diameter equals 2.5 cm and increases very slowly with distance, which is < 3 cm at 1 m distance from the second iris. The light is assumed to be nearly collimated.
   NOTE: The output from second iris should be uniform when checked by naked eyes.
3. Steer the collimated beam to a Lloyd's mirror interferometer. The Lloyd's setup contains a prism-based sample holder and a 5.04 cm mirror positioned perpendicular to it. The direct and reflected illuminations together create a stable standing wave along the sample surface for patterning. The prism acts as an antireflection device.
   NOTE: The period P of the standing wave can be written as: $P = \lambda/(2\sin\alpha)$, where λ = 325 nm and α is the incident angle with respect to sample normal, as is shown in **Figure 1**. The incident angle can be tuned by rotating the Lloyd's setup.

2. Periodic Array Preparation

NOTE: The sample is prepared under the standard procedure suggested by the manufacturer. All the procedures are performed at room temperature.

1. Use a 1 cm^2 glass substrate. Clean the glass with methanol and acetone for 10 min each in an ultrasonic bath and then pre-bake it on a hot plate at 200 °C for 1 h to remove dirt.
2. Spin-coat the glass substrate with a 5 nm thick adhesion layer and a 100 nm thick negative SU-8 photoresist with a two-speed spin-coater.
   1. Dilute the SU-8 photoresist with Gamma-Butyrolactone in a ratio of 1:5 (v/v) so that the thickness can be controlled close to 100 nm after spin-coating.

2. Dispense 3-5 drops (0.2 mL) of adhesion solution on the glass substrate and spin at 600 rpm for 10 s and 3600 rpm for 1 min, consecutively.
3. Repeat step 2.2.2 with 5-7 (0.3 mL) drops of diluted SU-8 from step 2.2.1 at the same speed.
   NOTE: The adhesion layer improves the adhesion between the glass substrate and the photoresist so that the photoresist would not peel off during developing. The thickness of the SU-8 layer is controlled by the concentration and the speed of spin-coater.

3. Prebake the sample on 65 °C and 95 °C hotplates for 1 min each. Ovens are not recommended here.
4. Transfer the sample to the prism in the interferometer. Add a drop of refractive index matching oil (n=1.45) to attach the sample on the prism. Place it as close to the mirror as possible.
   NOTE: The sample is attached on prism surface due to the surface tension of the oil. The refractive index of oil is chosen to be the same as prism and glass substrate to eliminate back reflection from the interference.
5. For a two-dimensional square lattice, expose the sample twice with the same exposure time but orthogonal directions; that is, expose the sample and then rotate it by 90° for the second exposure. When the photoresist is exposed to a 325 nm light, it crosslinks and cannot be dissolved by the SU-8 developer.
   NOTE: The diameter D of the array can be controlled by adjusting the exposure time.
6. Hard bake the sample at 65 °C and 95 °C for 2 min to prevent film cracking.
7. Immerse the whole sample in developer for 2 min with continuous agitation to dissolve the unexposed area.
8. Immerse the sample in isopropyl alcohol for 1 min to rinse the residuals and then dry it with compressed air. A nanohole array is then produced.

3. Gold Film Deposition and Light Emitter Coating

1. Attach the sample to the sample holder of the radio-frequency magnetron sputtering deposition system with double-sided tape for Au film deposition.
2. Pump down the chamber to a $2x10^{-6}$ Torr base pressure using a turbomolecular pump and then back fill it with $6x10^{-3}$ Torr ultra-high purity Ar gas.
3. Use a 5 cm diameter 99.9% Au target and place a shutter between the sample and the target. Use low power (50 W) to reduce the deposition rate as well as the surface roughness. With the shutter closed, pre-sputter the target for 10 min to remove dirt.
4. Open the shutter to process deposition at room temperature for 20 min. A film thickness of 100 nm is routinely deposited to ensure that the plasmonic system is optically thick with no transmission.
5. Once the sample is ready, spin-coat the light emitting materials such as organic dyes or quantum dots on the metal surface to form a thin layer of dielectrics.
   1. For the styryl 8 dye used in the reference[9], dissolve 20 µg of styryl 8 and 500 µg of polyvinyl alcohol polymer (PVA) in 5 mL of methanol.
   2. Dispense 3-5 drops (0.2 mL) of dye solution on the sample and spin at 600 rpm for 10 s and 3600 rpm for 1 min consecutively. The thickness is estimated to be 80 nm.
      NOTE: Water soluble or insoluble polymer can be used as anchoring material depending on the type of emitting material. However, the polymer should be non-emissive so that it would not interfere with the photoluminescence measurements. Polyvinyl alcohol polymer (PVA) is recommended for dissolving water-soluble dyes such as rhodamine 6G and styryl 8.

4. Reflectivity Measurements for Determining the SPP Decay Rates

NOTE: The polarization- and angle-resolved reflectivity spectroscopy setup is shown in **Figure 2**. It consists of a goniometer with three rotation stages for independently changing the sample orientation (stage 1) and detection angle (stage 2) as well as the sample azimuthal angle (stage 3).

1. Use a broadband white light from a quartz lamp as the light source. First couple it to a multimode fiber bundle and then collimate it by a pair of collinear face-to-face objective lenses (5X and 60X). Illuminate the light beam on the sample at different incident angles by changing sample orientation. Place a pair of incident polarizer and detection analyzer before and after the sample for polarization-dependent measurements.
   NOTE: The face to face objectives act as a lens system that collimates and expands the white light source from the multimode fiber.
2. Use a multimode fiber to collect the specular reflection from the sample, which is connected to a spectrometer and a CCD detector for spectroscopy.
3. Align the setup carefully to ensure both the sample orientation stage and detection rotation stages are concentric, *i.e.*, their rotation axes are collinear.
4. Calibrate the setup with a flat Au film. Measure the reflection spectra at different incident angles and compare them with the theoretical reflection spectra calculated by Fresnel equations using a known Au dielectric function. The two sets of data should be consistent with less than 5% of error.
5. Once the setup is ready, measure the linearly polarized, p or s, reflection spectra of the sample at different incident angles. The step size of the incident angle is 0.5° and the wavelength resolution is 0.66 nm. To collect the spectra under multiple incident angles, a control program is written for automation including the mechanical motion, shutter control, data acquisition, background subtraction, *etc*.
   NOTE: This step is done computationally. The program is available upon request. Please send an email to the corresponding author for the source code if needed.
6. Contour plot the reflectivity vs. wavelength and incident angle to obtain the dispersion relation of the plasmonic system for mode identification and decay rate determination.
   NOTE: The sample azimuthal angle is to locate the position in the Brillouin zone. For example, for square lattice sample, rotate the sample azimuthally so that one of its periods is parallel with the incident plane and this defines the Γ-X direction. Rotate the sample by 45° to define the Γ-M direction.

7. If the incident polarized is set at 45° with respect to the incident plane and the analyzer is at -45°, measure the orthogonal, or cross-polarized, reflectivity mapping.
8. Extract the p-polarized and orthogonal reflection spectra and fit them by using CMT[9,12,13], as described in the Discussion to determine the decay rates of SPPs.

5. Photoluminescence Measurements for Determining the Emission Power Ratio

Note: The angle- and polarization-resolved photoluminescence setup is shown in **Figure 3**.

1. Replace the broadband light source with 514 nm argon ion or 633 nm HeNe laser. Use a laser line filter with a full width half maximum (FWHM) less than 5 nm to clean the laser spectrally and place a half-wave plate to control the polarization state of the laser beam. The goniometer and the detection unit remain unchanged. Place a notch filter before the detection unit to remove the laser line, which buries the luminescence.
   NOTE: The wavelength of the laser depends on the type of emitting materials. Higher photon energy is required to excite the material with shorter emission wavelength.
2. To measure the emission power ratio for Eq. (2) & (3), conduct two types of measurements: the detection and incident scans. The interplay between the incident and detection scans assist in determining P_d^w, $P_d^{w/o}$, $P_{SPP}^{\vec{k}_{SPP},\alpha}$, and P_d.
3. For the incident scan, vary the incident angle continuously but fix the detection angle with respect to the sample normal.
   NOTE: This step is done computationally. This configuration selectively excites the incoming SPPs, which are incident angle dependent, while monitoring the variation of the emission under the chosen detection angle. In other words, the emission increases when the incident angle fulfills the phase matching equation in Eq. (1).
   1. Contour plot the photoluminescence spectra against wavelength and the incident angle for the incident scan mapping. Measure the mappings for different detection angles but the relative intensities are found the same. Therefore, the incident scan probes the effect of the incoming SPPs on the emission or simply the excitation enhancement, which allows us to measure P_d^w and $P_d^{w/o}$.
4. For the detection scan, fix the incident angle with respect to the sample normal but vary the detection angle.
   NOTE: This step is done computationally.
   1. Similarly, contour plot the photoluminescence spectra with wavelength and detection angle yields the detection scan mapping. As the SPP emission arises from the radiation damping of SPPs, the emission is strongly detection angle dependent. Therefore, under constant excitation, the emission increases when the detection angle fulfills Eq. (1). This configuration probes the emission enhancement and allows us to determine $P_{SPP}^{\vec{k}_{SPP},\alpha}$ for different α^{th} order as long as it has well-defined detection angle dependence.

Representative Results

An example of an Au periodic array is given in the inset of **Figure 4a**[8]. The plane view SEM image shows that the sample is a 2D square lattice circular hole array with a period of 510 nm, a hole depth of 280 nm, and a hole diameter of 140 nm. The p-polarized reflectivity mapping taken along the Γ-X direction is shown in **Figure 4a**. The dash line is calculated by the phase matching equation Eq. (1) indicating that (m = -1, n = 0) SPPs are excited.

When the polarizer and analyzer are set at orthogonal positions, the corresponding reflectivity mapping is shown in **Figure 4b**. We see that the mapping is almost identical to the linear polarized mapping except the background now becomes zero as the non-resonant reflection is removed by the analyzer. In addition, the reflectivity profiles are changed from dips to peaks as only the SPP radiation damping remains after the removal of the background.

In fact, the dispersion relation is a good tool for studying SPMF. Assuming the laser excitation wavelength is 700 nm, incoming SPPs will be generated at a 19° incident angle and they will interact with the emitters if their absorption band matches. On the other hand, SPP emission will be detected at a 23° incident angle if the emission occurs at 730 nm. Therefore, the SPP resonances allow us to excite the incoming SPPs for excitation enhancement and to locate the outgoing SPPs for emission enhancement.

We spin coat CdSeTe quantum dots doped PVA polymer on the array[10]. **Figure 5a & 5b** display the p-polarized and orthogonal reflectivity mapping taken along the along the Γ-X direction, showing the (-1,0). **Figure 5c & 5d** shows the corresponding photoluminescence incident and detection scan mappings taken at the detection and incident angles of 0° and 0°, respectively. The laser wavelength λ_{ex} is 633 nm. In fact, consistent with the reflectivity mapping, we see that strong emission occurs at an incident angle of 18.5° where the incoming (-1,0) SPPs are excited. On the other hand, from the detection scan, the strong resemblance between the reflectivity and the photoluminescence verifies that the emissions are enhanced when the outgoing SPPs are excited.

The determination of the excitation and coupling rates requires the SPP decay rates and photoluminescence power ratios[10]. To determine the decay rates at 633 nm along the Γ-X direction, the p-polarized and orthogonal reflectivity spectra extracted from **Figure 5a & 5b** are shown in **Figure 6a**. The p-polarized spectrum shows a Fano-like profile that can be described as $\left| r_p + \frac{\Gamma_{rad}}{i(\omega - \omega_{SPP}) + \Gamma_{tot}/2} \right|^2$, where r_p is the nonresonant reflectivity and ω_{SPP} is the resonant photon energy, whereas the orthogonal counterpart follows $\frac{1}{4}\frac{(\Gamma_{rad})^2}{(\omega-\omega_{SPP})^2+(\Gamma_{tot}/2)^2}$, exhibiting a Lorentzian lineshape[12]. They are then best fitted and the total and radiative decay rates, Γ_{tot} and Γ_{rad}, are 95.08 and 27.15 meV (with *h*).

On the other hand, the photoluminescence power ratio is obtained as follows. From the incident scan in **Figure 5c**, the emission profile at the emission wavelength λ_{em} = 690 nm, where the direct emission locates, is extracted in **Figure 6b**. The power ratio $P_d^w/P_d^{w/o}$, which is defined as the direct emission with and without the incoming SPPs, simply is the intensity at 18.5° divided by the flat background (6.896). Γ_{ex}/η is then determined to be 574.04 meV.

On the other hand, the coupling rate is emission wavelength dependent. The emission wavelength at 690 nm is chosen as an example. The total and radiative decay rates, Γ_{tot} and Γ_{rad}, are 60.06 and 17.12 meV (with *h*), respectively. The detection scan profile is extracted from **Figure 5d** and displayed in **Figure 6c**. The power ratio $P_{SPP}^{(-1,0)}/P_d$ is defined as the (-1,0) SPP emission divided by the half-space direct emission assuming that the sample has no transmission. Since the detector covers a solid angle $\Delta\Omega \sim \pi^3/720^2$ sr, for a Lambertian surface, $P_d = \pi b/\Delta\Omega$, where b follows the background in **Figure 6c** as $b\cos\theta_{detection}$. On the other hand, the $P_{SPP}^{(-1,0)}$ is given as the peak profile divided by $\Delta\Omega$. As a result, Γ_c/Γ_r is found to be 0.805.

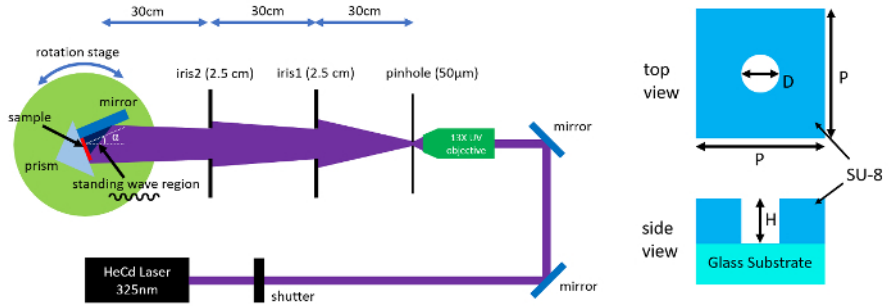

Figure 1. Schematic of interference lithography. A 325 nm laser light focused through a spatial filter and then is illuminated on a Lloyd's mirror interferometer where the sample is located. The standing wave forms along the sample surface for exposure. Inset: schematics of the top and side view of the sample completed in section 2. Please click here to view a larger version of this figure.

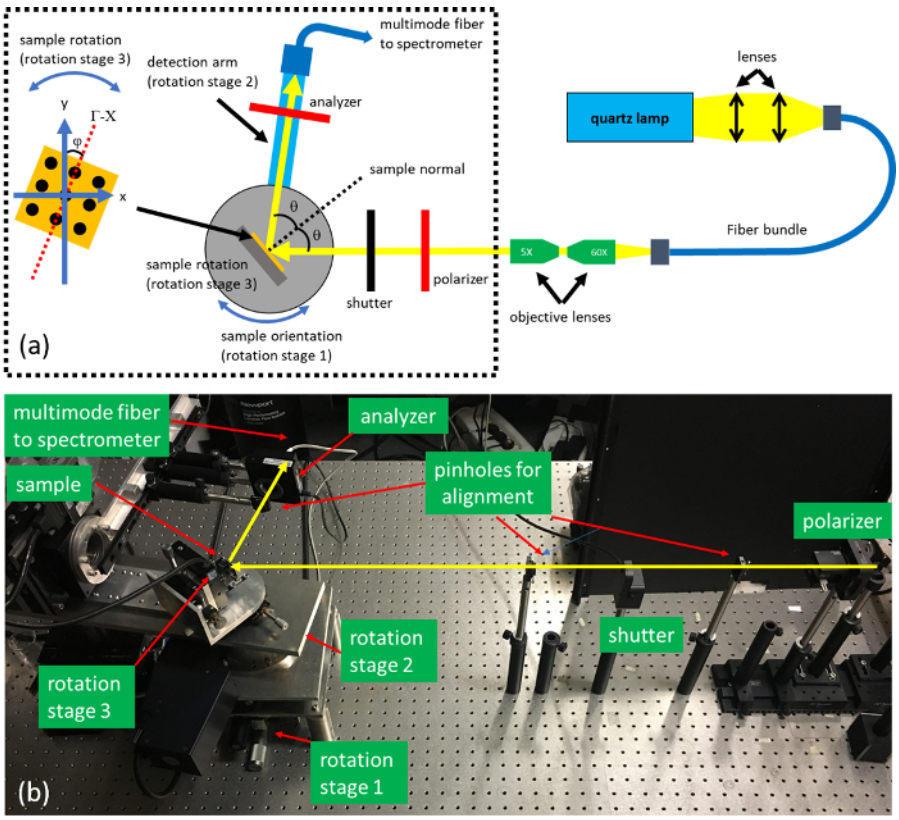

Figure 2. Polarization- and angle-resolved reflectivity spectroscopy. (**a**) Schematics of polarization- and angle-resolved reflectivity spectroscopy. Three rotation stages are used for constructing the goniometer. A multimode fiber coupled spectrometer and CCD detector is used for detection. A broadband white light source is used for reflectivity measurements. (**b**) Real-life image of the major part (black dash box in (**a**)) of the polarization- and angle-resolved reflectivity spectroscopy. Please click here to view a larger version of this figure.

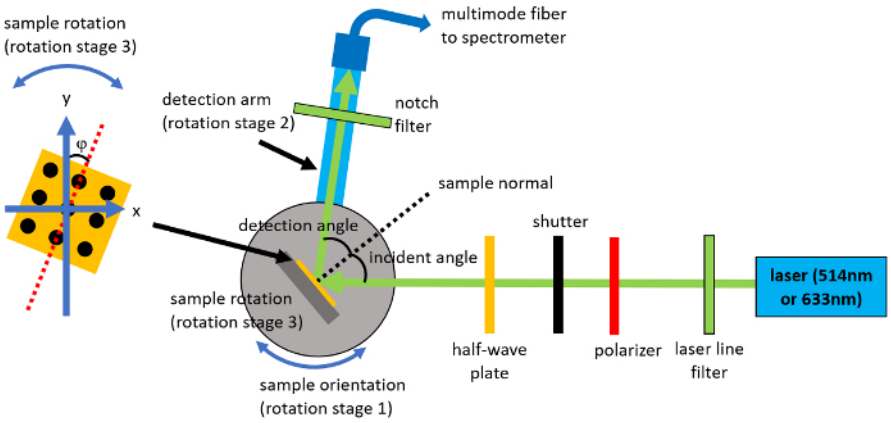

Figure 3. Schematics of polarization- and angle-resolved photoluminescence spectroscopy. A 514 or 633 nm laser is used for photoluminescence. Please click here to view a larger version of this figure.

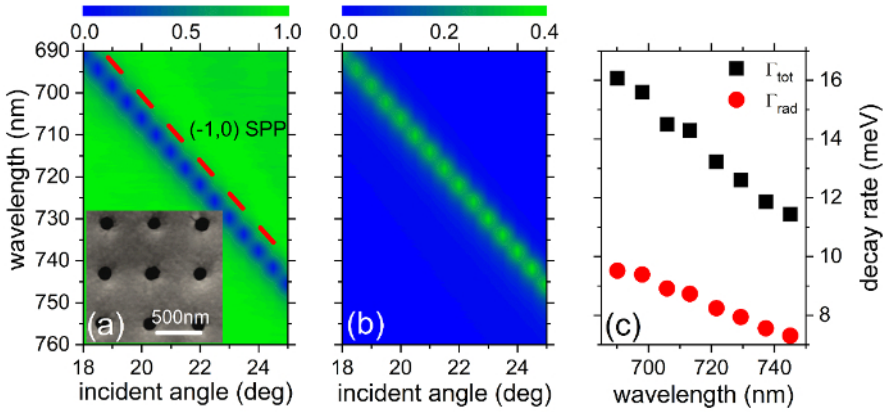

Figure 4. Reflectivity mappings and deduced decay rates. (**a**) The p-polarized reflectivity mapping of an Au array taken along the Γ-X direction. The dash line is calculated by using the phase matching equation, showing (-1,0) SPPs are excited at different wavelengths. Inset: the plane-view SEM image of the array. (**b**) The corresponding orthogonal reflectivity mapping showing that the background is nulled and the reflectivity dips now become peaks. (**c**) The plot of Γ_{tot} and Γ_{rad} as a function of wavelength. The results are reproduced from reference[9]. Please click here to view a larger version of this figure.

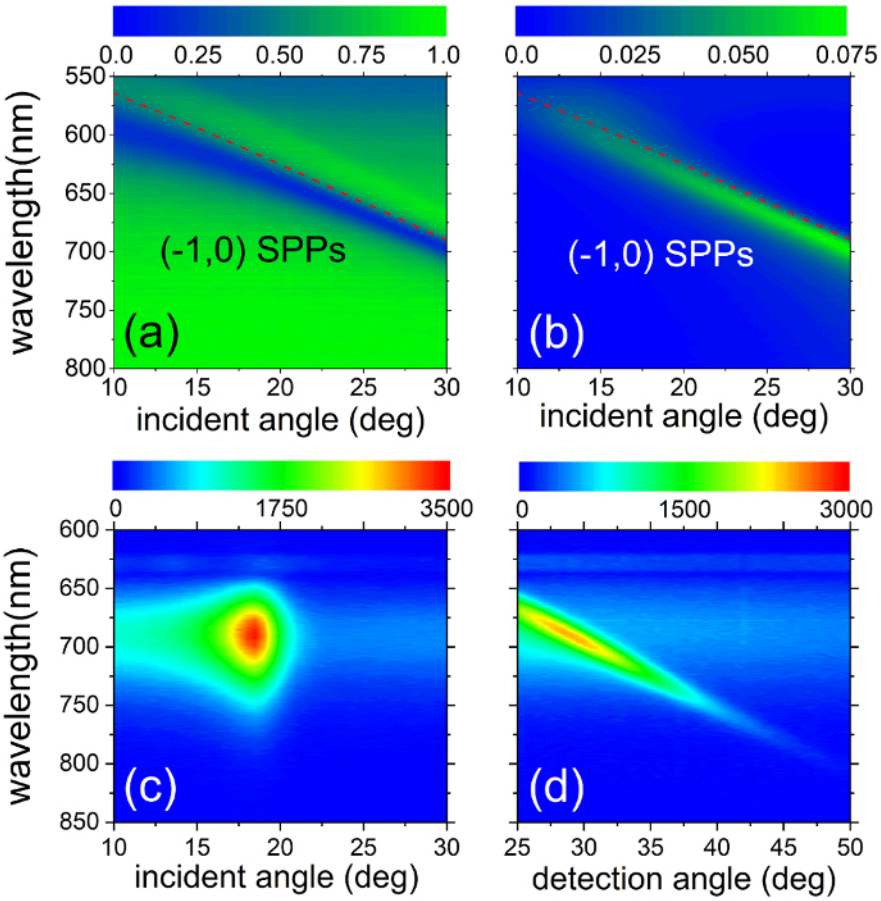

Figure 5. The reflectivity, incident and detection scan mappings of an array coated with CdSeTe quantum dots taken along the Γ-X direction. The (**a**) p-polarized and (**b**) orthogonal reflectivity mappings and the corresponding photoluminescence (**c**) incident and (**d**) detection scan mappings taken at detection and incident angle = 0° and 0°, respectively. The laser wavelength λ_{ex} is 633 nm. The results are reproduced from reference[10]. Please click here to view a larger version of this figure.

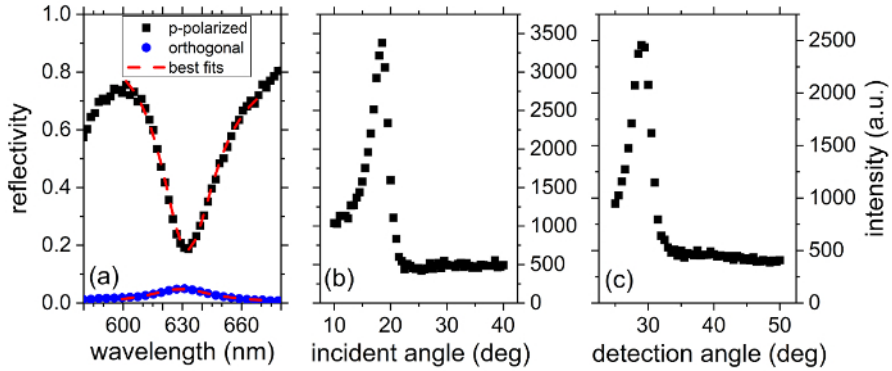

Figure 6. Representative reflectivity, incident and detection scan profile. (**a**) The p-polarized and orthogonal reflectivity spectra together with the best fits for determining Γ_{tot} and Γ_{rad} at 633 nm. (**b**) The extracted (**b**) incident and (**c**) detection scan profiles. The results are reproduced from reference[10]. Please click here to view a larger version of this figure.

Discussion

In this protocol, there are several critical steps. First, mechanical stability is crucial in sample preparation. The standing wave generated by Lloyd's setup is sensitive to the phase difference between two illumination beams. Therefore, any vibration during the exposure time will degrade the uniformity and edge sharpness of the nanohole. It is highly recommended to operate in a vibration-free environment, *e.g.*, an optical table with vibration isolation supports. In addition, high power laser is also desired to minimize vibration as it reduces exposure time accordingly. Second, the pinhole in step 1.1 must be chosen properly. The hole size should be small enough to perform mode cleaning on one side and still large enough to transmit sufficient power for exposure on the other side. We recommend a 50 μm pinhole and 13X objective for the HeCd multimode laser. Third, it is noted that the Lorentzian line shape of orthogonal reflectivity is valid only

when $r_p \approx r_s$, where r_p and r_s are non-resonant reflectivity for p- and s-polarized illumination[12]. However, for a nanohole array with glancing incident angle or some anisotropic metamaterials, the difference between r_p and r_s cannot be neglected and the resulting reflectivity yields $\frac{1}{4}\left|r_p - r_s + \frac{\Gamma_{rad}}{i(\omega - \omega_{SPP}) + \Gamma_{tot}/2}\right|^2$, giving rise to Fano lineshape.

In summary, this protocol describes a method to determine the excitation and coupling rates between the light emitters and SPPs from 2D metallic periodic arrays. The rate is measured by angle- and polarization-resolved reflectivity and photoluminescence spectroscopy, both of which are frequency domain techniques. Compared with conventional time-resolved techniques, this method not only differentiates the excitation and decay processes of SPMF, which are not considered in most fluorescence enhancement studies, but also determines the coupling rates of light emitters to different SPP modes. As time-resolved techniques only measure the total lifetime of a light emitter and are unable to identify the contributions from different resonant modes, our method would certainly add value to this field especially when light emitters are being placed in a complex resonance system. For a periodic plasmonic system, $\vec{k}_{spp,\alpha}$ mode has a well-defined decay direction whereas direct emission is assumed to be isotropic. Their differences in emission direction give rise to the mode identification. As directional emission is a universal behavior in nanomaterials, such differentiation can be easily extended to other resonant systems like metamaterials and photonic crystals. We anticipate this technique to be an enabling technology for studying fluorescence enhancement between light emitters and resonant cavities.

Disclosures

The authors declare that they have no competing financial interests.

Acknowledgements

This research was supported by the Chinese University of Hong Kong through the Direct Grants 4053077 and 4441179, RGC Competitive Earmarked Research Grants, 402812 and 14304314, and Area of Excellence AoE/P-02/12.

References

1. Okamoto, K., *et al.* Surface-plasmon-enhanced light emitters based on InGaN quantum wells. *Nature Materials.* **3** (9), 601-605 (2004).
2. Akselrod, G.M., *et al.* Leveraging Nanocavity Harmonics for Control of Optical Processes in 2D Semiconductors. *Nano Letters.* **15** (5), 3578-3584 (2015).
3. Gontijo, I., *et al.* Coupling of InGaN quantum-well photoluminescence to silver surface plasmons. *Physical Review B.* **60** (16), 11564 (1999).
4. Huang, K.C.Y., *et al.* Antenna electrodes for controlling electroluminescence. *Nature Communications.* **3**, 1005 (2012).
5. Atwater, H.A., Polman, A. Plasmonics for improved photovoltaic devices. *Nature Materials.* **9** (3), 205-213 (2010).
6. Anker, J.N., *et al.* Biosensing with plasmonic nanosensors. *Nature Materials.* **7** (6), 442-453 (2008).
7. Chen, Y., *et al.* Excitation enhancement of CdSe quantum dots by single metal nanoparticles. *Applied Physics Letters.* **93** (5), 053106 (2008).
8. Birowosuto, M.D., Skipetrov, S.E., Vos, W.L., Mosk, A.P. Observation of Spatial Fluctuations of the Local Density of States in Random Photonic Media. *Physical Review Letters.* **105** (1), 013904 (2010).
9. Cao, Z.L., Ong, H.C. Determination of coupling rate of light emitter to surface plasmon polaritons supported on nanohole array. *Applied Physics Letters.* **102** (24), 241109 (2013).
10. Lin, M., Cao, Z.L., Ong, H.C., Determination of the excitation rate of quantum dots mediated by momentum-resolved Bloch-like surface plasmon polaritons. *Optics Express.* **25** (6), 6029-6103 (2017).
11. Nikolaev, I.S., Lodahl, P., Driel, A.F.V., Koenderink, A.F., Vos W.L. Strongly nonexponential time-resolved fluorescence of quantum-dot ensembles in three-dimensional photonic crystals. *Physical Review B.* **75** (11), 115302 (2007).
12. Cao, Z. L., Lo, H. Y., Ong, H. C., Determination of absorption and radiative decay rates of surface plasmon polaritons from nanohole array. *Optics Letters.* **37** (24), 5166-5168 (2012).
13. Haus, H.A. *Waves and Fields in Optoelectronics.* Prentice-Hall, Englewood Cliffs, N.J. (1984).

